

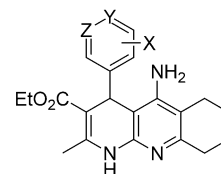
DOI: 10.1002/cmdc.201100239

Chemical and Pharmacological Studies on Enantiomerically Pure *p*-Methoxytacriprines, Promising Multi-Target-Directed Ligands for the Treatment of Alzheimer's Disease

Manuela Bartolini,^[a] Marco Pistolozzi,^[a] Vincenza Andrisano,^[a] Javier Egea,^[b, c, d] Manuela G. López,^[b, c, d] Isabel Iriepa,^[e] Ignacio Moraleda,^[e] Enrique Gálvez,^[e] José Marco-Contelles,^[*f] and Abdelouahid Samadi^[f]

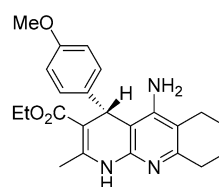
Alzheimer's disease (AD) is an age-related neurodegenerative process characterized by progressive memory loss and other cognitive impairments.^[1] Although the etiology of AD is not well known, several factors such as amyloid- β (A β)^[2] deposits, τ -protein aggregation, oxidative stress or low levels of acetylcholine^[3] are thought to play significant roles in the pathophysiology of the disease.^[4] In spite of the continuous efforts of the pharmaceutical industry and academia, an efficient strategy for the treatment of AD is still lacking. This is partially related to the complexity of the pathology, in which multiple factors contribute to the final scenario. The multifactorial nature of AD has given rise to the rational basis for the development of the most current innovative therapeutic approaches based on the "one molecule, multiple targets" paradigm.^[5–9] The multitarget approach^[10] has been widely explored leading to the development of several multi-target-direct ligands (MTDLs), which include novel tacrine–melatonin hybrids,^[11] dual inhibitors of acetylcholinesterase (AChE) and monoamine oxidase,^[12] or serotonin transporters,^[13] potent cholinesterase inhibitors with antioxidant and neuroprotective properties,^[14] gallamine–tacrine hybrids binding at cholinesterases and M₂ muscarinic receptors,^[15] or NO-donor–tacrine hybrids as hepatoprotective anti-AD drugs.^[16]

Based on the multitarget approach, some years ago we designed and synthesized novel multipotent molecules, called ta-

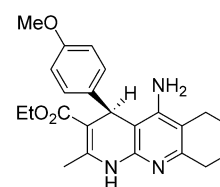


X = H, 4'-F, 2'-CF₃, 2'-NO₂, 3'-NO₂, 4'-NO₂, 4'-Me, 4'-C₆H₅, 2'-OMe, 3'-OMe, 4'-OMe, 3', 4'-di-OMe
Y = CH, C, N; Z = CH, N

Tacriprines (I)



(*R*)-*p*-Methoxytacriprine [(*R*)-1]



(*S*)-*p*-Methoxytacriprine [(*S*)-1]

criprines (I), by combination of tacrine and nimodipine, as reference agents with a multipotent cholinergic and calcium antagonism profile, respectively, for the treatment of AD.^[17,18] Racemic tacriprines exhibited potent and selective AChE inhibition, high calcium-channel blocking activity, as well as neuroprotective/antioxidant properties, able to cross the blood–brain barrier.

Particularly, (*R/S*)-*p*-methoxytacriprine (ethyl 5-amino-4-(4-methoxyphenyl)-2-methyl-1,4,6,7,8,9-hexahydrobenzo[*b*][1,8]naphthyridine-3-carboxylate; (*R/S*)-1), one of the most potent cholinergic tacriprines (IC₅₀ = 105 ± 15 nM against human AChE), at 100 μM showed 30.7 ± 8.6% inhibition of the pro-aggregating action of AChE on A β peptide (230 μM); furthermore, (*R/S*)-1 was also a moderate inhibitor of β -amyloid self-aggregation (34.9 ± 5.4% at [I] = 50 μM).^[18] Overall, these results prompted us to consider 1 as an appropriate hit compound in this project, and consequently, to undertake the pharmacological analysis of both enantiomers. The detailed investigation of chiral discrimination has enormous importance in medicinal chemistry as a means to better elucidating the mechanisms of interaction and to identify structural features involved in ligand–target recognition.

The synthesis of (*R/S*)-1 was scaled up for this study, but essentially followed the general protocol previously described.^[18] Briefly, starting from a mixture of *E/Z*-isomers of ethyl 2-(4-methoxybenzylidene)-3-oxobutanoate (2),^[19] and reacting it with

[a] Dr. M. Bartolini, Dr. M. Pistolozzi, Prof. V. Andrisano
Department of Pharmaceutical Sciences, University of Bologna
Via Belmeloro 6, 40126 Bologna (Italy)
Fax: (+39) 051-2099734
E-mail: manuela.bartolini3@unibo.it

[b] Dr. J. Egea, Prof. M. G. López
Instituto Teófilo Hernando
C/ Arzobispo Morcillo 4, 28029 Madrid (Spain)

[c] Dr. J. Egea, Prof. M. G. López
Departamento de Farmacología y Terapéutica, Universidad Autónoma de Madrid
C/ Arzobispo Morcillo 4, 28029 Madrid (Spain)

[d] Dr. J. Egea, Prof. M. G. López
HIV Unit, Instituto de Investigación Hospital Universitario La Paz (IdiPAZ)
Autónoma University School of Medicine,
Pº de la Castellana 261, 28046 Madrid (Spain)

[e] Prof. I. Iriepa, I. Moraleda, Prof. E. Gálvez
Departamento de Química Orgánica, Universidad de Alcalá
Ctra. Madrid-Barcelona, Km. 33,6, 28871 Alcalá de Henares, Madrid (Spain)

[f] Prof. J. Marco-Contelles, Dr. A. Samadi
Laboratorio de Radicales Libres y Química Computacional (IQOG, CSIC)
C/ Juan de la Cierva 3, 28006-Madrid (Spain)
E-mail: iqoc21@iqog.csic.es

Supporting Information for this article is available on the WWW under <http://dx.doi.org/10.1002/cmdc.201100239>.

3,3-diaminoacrylonitrile,^[20] prepared in situ from ethyl cyanoacetimidate hydrochloride (**3**)^[21] (see scheme S1, Supporting Information), the resulting ethyl (\pm)-ethyl 6-amino-5-cyano-4-(4-methoxyphenyl)-2-methyl-1,4-dihydropyridine-3-carboxylate (**4**) was isolated in 56% yield. Next, a Friedländer-type reaction^[22–24] between the key β -enamionitrile **4** and cyclohexanone (aluminum trichloride, 1,2-dichloroethane, microwave irradiation) provided the desired target molecule **1** in significantly higher yield (92%) than that obtained under standard conditions, heating at reflux for a long period, described previously.^[18]

Chiral resolution of (*R/S*)-**1** was carried out by semipreparative high-performance liquid chromatography (HPLC) using a chiral stationary phase, which allowed the isolation of two fractions in high enantiomeric excess (*ee* > 98%).^[18] **A** $\{[\alpha]_D = +179$ (*c* = 0.5, CHCl₃), and **B** $\{[\alpha]_D = -180$ (*c* = 0.62, CHCl₃). Determination of the absolute configuration at C4 in enantiomers **A**^[25] and **B**^[26] was achieved using the hydrochloride salts, which gave excellent crystals for X-ray diffraction analyses. Thus, it was unequivocally established that isomer **A** has the *R* absolute configuration at C4, while isomer **B** has the *S* absolute configuration at C4 (see figures S1 and S2, respectively, Supporting Information). The inhibitory activity against AChE was previously and preliminary tested^[18] and re-evaluated here before further studies (see table S3, Supporting Information). *K_i* values for the inhibition of *Electrophorus electricus* AChE (EeAChE) were also obtained for both enantiomers and the racemate (*R/S*)-**1** (Table 1). Results confirmed that chirality at the stereocenter C4 modulates the inhibitory activity against both cholinesterase enzymes. Specifically, the inhibitory activity of enantiomer (*S*)-**1** resulted approximately tenfold higher than that of (*R*)-**1**, showing an inhibitory constant in the low nanomolar range (*K_i* = 16.1 ± 1.9 nM, Table 1) against EeAChE. Both enantiomers were selective AChE inhibitors, however, the activity profile of the two enantiomers against human butyrylcholinesterase (hBuChE) followed an opposite trend, with the *R* enantiomer at least one order of magnitude more potent on hBuChE than the *S* enantiomer (see table S3, Supporting Information).

With a view to developing a new disease-modifying drug able to interfere with the proaggregating action of AChE on amyloid peptides, likely exerted through the interaction of A β with the peripheral binding site (PAS) of the enzyme,^[27,28] the mechanisms of action of (*R*)- and (*S*)-**1** were investigated by Ellman's method^[29] using EeAChE as the target enzyme. Lineweaver–Burk reciprocal plots obtained with (*R*)- and (*S*)-**1** showed both decreased *v_{max}* and higher *K_m* values at increasing inhibitor concentrations, which indicates mixed-type inhibition arising from significant inhibitor interaction with both the free and the acetylated enzyme (see figure S3, Supporting Information).

The assessment of the absolute configuration of the pure enantiomers by X-ray analysis also allowed a re-investigation of the molecular docking simulation. Ligand docking studies were performed with hAChE (PDB: 1B41) using AutoDock Vina.^[8] To account for side chain flexibility during docking, flexible torsion angles in the ligands were assigned, and the acyclic dihedral angles were allowed to rotate freely. Besides, Trp286, Tyr124, Tyr337 and Tyr72 receptor residues were selected to keep flexible during docking simulation. To ensure the accuracy of our docking experiments, we first compared several known crystal structures of ligand-bound *Torpedo californica* AChE (TcAChE) with their respective docking structure. These successful trial runs involved Protein Data Bank (PDB) data obtained from co-crystallizations of TcAChE with known ligands, tacrine, donepezil, galanthamine and bis-tacrine AA71536. This set of AChE active site ligands was chosen in order to span the molecular diversity of the ligands. Computational docking studies of (*S*)-**1** with hAChE yielded two major predicted binding modes at the binding/active site of the enzyme given that (*R*)-**1** is a mixed inhibitor. Figure 1 illustrates the two most energetically favorable predicted binding modes of (*S*)-**1** at the active site of hAChE. Mode I places the ligand deep in the binding pocket next to the residues involved in catalysis (Ser203, Glu334 and His447), although it does not directly interact with them (Figure 1a). Mode II places the ligand in the PAS; in this orientation, the indole ring of Trp286 forms a π – π interaction with the *p*-methoxyphenyl ring. The ligand–enzyme

interaction is predicted to be further strengthened by a hydrogen bond between the amino group of (*S*)-**1** and the carboxylate group of Asp74. These data suggest that (*S*)-**1** can be accommodated in both the PAS and the central anionic site (CAS).

For (*R*)-**1**, three binding modes were predicted: Mode I, the most energetically favored binding mode, places the ligand in the opening of the PAS and the tacrine-like moiety stacks against the indole ring of Trp286 (Figure 2a). The pyridine nitrogen is also predicted to mediate a hydrogen-bond interaction with

Table 1. Inhibition of hAChE-mediated A β _{1–40} aggregation and A β _{1–42} self-aggregation by racemic *p*-methoxytacrinyne (**1**) and its enantiomers.

Compd	<i>K_i</i> ^[a] [nM] EeAChE	hAChE-induced A β _{1–40} aggregation		A β _{1–42} self-aggregation	
		Inhibition ^[b] [%]		Inhibition ^[c] [%]	IC ₅₀ [μ M]
Tacrine	nd	7 ^[d]		4.4 ± 1.9	nd
(<i>R/S</i>)- 1	58.0 ± 5.0	30.7 ± 8.6		34.9 ± 5.4 ^[e]	nd
(<i>R</i>)- 1	125 ± 22	25.1 ± 5.3		84.1 ± 6.2	29.9 ± 1.7
(<i>S</i>)- 1	16.1 ± 1.9	28.7 ± 4.5		88.6 ± 4.2	33.2 ± 4.3

[a] Estimates of the competitive inhibition constants (*K_i*) were obtained from replots of the slopes of the Lineweaver–Burk graphs versus inhibitor concentration determined as reported in the Supporting Information. [b] Percentage of ThT fluorescence reduction caused by inhibitors at 100 μ M. [A β _{1–40}] = 230 μ M, [hAChE] = 2.3 μ M. Values are the mean ± SEM of two experiments performed in duplicate. [c] Percentage of ThT fluorescence reduction caused by inhibitors at 50 μ M. [A β _{1–42}] = 50 μ M. Values are the mean ± SEM of three independent experiments, each carried out in duplicate. [d] Datum from Reference [30]. [e] Datum from Reference [18]. nd = not determined.

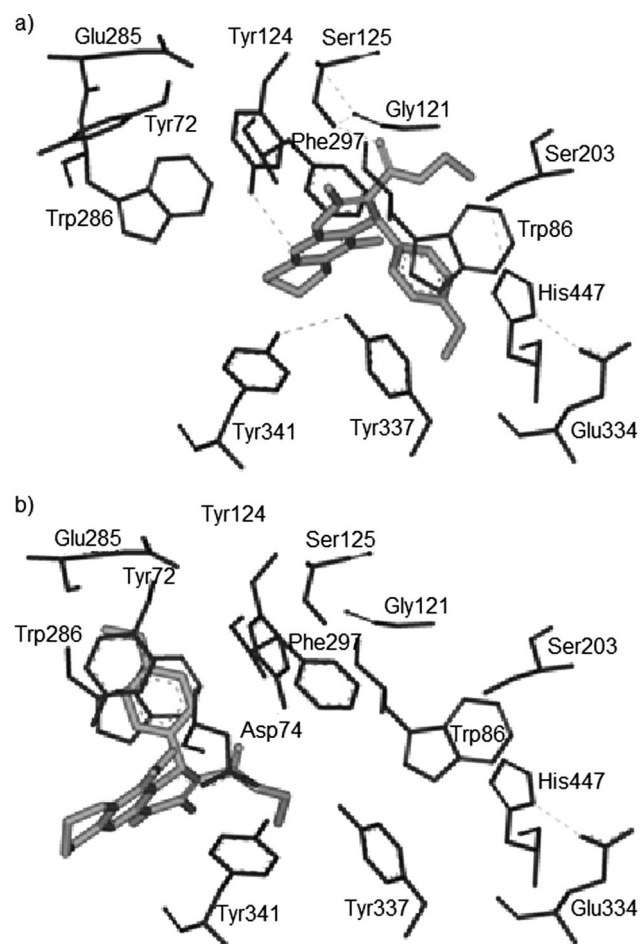


Figure 1. Two major binding modes of (*S*)-1 to hAChE predicted by docking simulations. a) Mode I: first of eight binding modes; binding affinity = $-7.3 \text{ Kcal mol}^{-1}$; the position of (*S*)-1 within the CAS is shown. b) Mode II: second of eight binding modes; binding affinity = $-7.1 \text{ Kcal mol}^{-1}$; the position of (*S*)-1 within the PAS is shown. The compound is rendered as sticks and illustrated in blue. The hydrogen bonds are represented as pink dashed lines.

the hydroxy group of Tyr124. Mode II and mode III place the ligand within the central region of the active site gorge with occupation to the choline binding site, although no interactions with the catalytic triad residues have been found (Figure 2b). These data suggest that this ligand is also able to interact with the CAS of hAChE but to a lesser extent than with the PAS.

In summary, enantiomers (*S*)-1 and (*R*)-1 have the ability to bind to both binding sites of hAChE; this explains their mixed-type inhibiting properties. The geometrical and energetically features of the (*S*)-1–enzyme complexes contribute to the higher affinity of (*S*)-1 and made it a more potent inhibitor than (*R*)-1.

The two enantiomers were also docked to the hBuChE (major binding modes are given in figure S6 and S7, Supporting Information). Docking studies confirmed an opposite trend for (*R*)-1 and (*S*)-1 in complex with hBuChE as compared with hAChE; this is in agreement with the selectivity trend observed

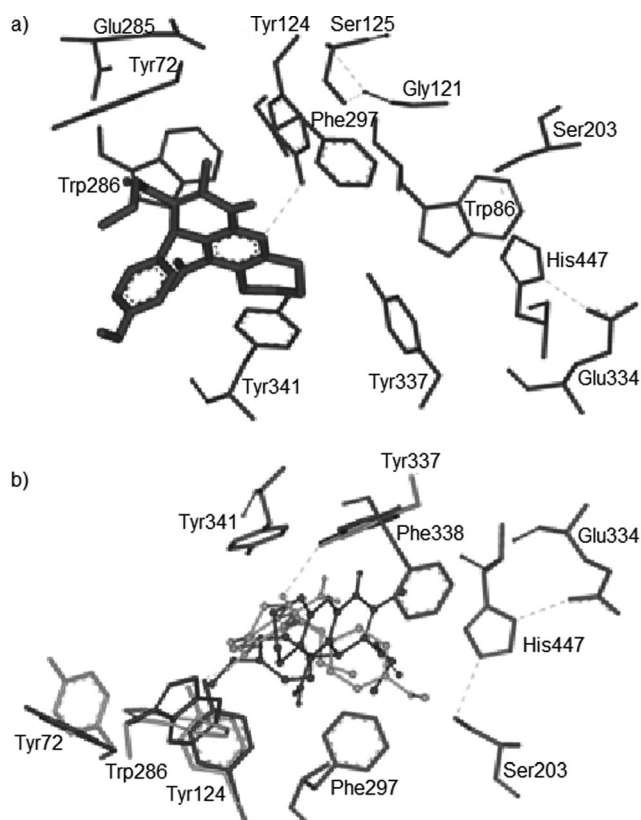


Figure 2. Predicted binding modes of (*R*)-1 at the active site of AChE: a) Mode I: first of 13 binding modes; binding affinity = $-6.3 \text{ Kcal mol}^{-1}$; b) Overlay of modes II and III; Mode II: third of 13 binding modes (red); binding affinity = $-4.2 \text{ Kcal mol}^{-1}$; Mode III: 12th of 13 binding modes (blue); binding affinity = $-3.3 \text{ Kcal mol}^{-1}$. Residues that change their orientation in both poses are illustrated in the same color that the corresponding ligand. The hydrogen bonds are represented as pink dashed lines.

for the two enantiomers in Ellman's assay (see table S3, Supporting Information).

On the basis of the proposed ability of both enantiomers to interact with the PAS of AChE, which is thought to play a central role in promoting A β aggregation,^[27,28] their ability to inhibit amyloid aggregation induced by hAChE was evaluated using a thioflavin T (ThT)-based assay.^[30] Indeed, AChE co-localizes with amyloid plaques, and the interaction of A β soluble peptides with AChE PAS is thought to trigger amyloid aggregation.^[27,28,31] A recently developed fluorescent coumarin–tacrine hybrid, able to interact with both the CAS and PAS, further confirmed the role of the PAS in amyloid aggregation.^[32]

Data showed that both enantiomers exhibit a similar inhibitory activity (Table 1) ranging from 25 to 29% (at $[I] = 100 \mu\text{M}$, $[A\beta] = 230 \mu\text{M}$), which did not significantly differ from the racemic mixture. This suggests that aggregation inhibition is not sensitive to the chirality of the inhibitors, as expected from kinetic and molecular modeling investigations, which showed that the two enantiomers are similarly able to interact with the PAS. In this respect, the fact that tacrine did not show significant inhibitory activity against hAChE-induced A β aggregation might be attributed to the higher affinity of tacrine for the CAS over the PAS. The major difference between tacrine and 1

is the larger size of **1** due to the *p*-methoxyphenyl ring. This moiety increases the affinity of (*R*)-**1** and (*S*)-**1** for the PAS compared with tacrine. As for the racemate (*R/S*)-**1**, the inhibitory activities of the individual enantiomers of *p*-methoxytacirpyrine were higher than that of donepezil^[30] and similar to that of AP2238.^[33]

Amyloid aggregates are widely believed to be acute mediators of cognitive impairment.^[34] Therefore, the ability of (*R*)-**1** and (*S*)-**1** to directly inhibit $A\beta_{1-42}$ self-aggregation was investigated by a ThT-based assay^[35,36] and transmission electron microscopy (TEM). (*R*)-**1** and (*S*)-**1** showed strong inhibition with values of 84.1 ± 6.2 and 88.6 ± 4.2 %, respectively, at 1:1 molar ratio with $A\beta$, while a weaker inhibitory potency was observed for the racemate (*R/S*)-**1**.

The inhibitory action of the single enantiomers at $50 \mu\text{M}$ was in the same range as propidium (89.8%)^[37] and bis(7)tacrine (71.2%).^[38] It should also be noted that tacrine, as well as other marketed drugs for the treatment of AD such as galanthamine and rivastigmine, does not show any significant antiaggregating properties (inhibition $< 10\%$). In agreement with data obtained in the ThT-based assay, TEM images showed that no amyloid fibrils were formed when $A\beta_{1-42}$ was incubated for 24 h with single enantiomers in a 1:1 molar ratio (Figure 3c and d), while a large amount of ordered amyloid fibrils appeared in the absence of inhibitor (Figure 3a), further confirming the ability of both enantiomers to strongly inhibit amyloid fibril formation. The weaker inhibitory activity of (*R/S*)-**1** and reconstituted racemic mixture obtained in the ThT-based assay ($45.8 \pm 2.4\%$ and $49.5 \pm 1.0\%$, respectively, at $50 \mu\text{M}$) was also confirmed by TEM (Figure 3b), which showed the formation of a few small aggregates when $A\beta_{1-42}$ was incubated with (*R/S*)-**1**. Structural or conformational alterations in the aggregation assay conditions were excluded by circular dichroism (CD/UV)

analyses (figure S4 and S5, Supporting Information). Although fluorescence and electron microscopy analyses gave congruent data, the inhibition profile obtained for (*R/S*)-**1** versus individual enantiomers cannot be definitively explained. However, obtained data generally point towards a role of chirality in the inhibition of amyloid aggregation. On the other hand, the sporadic data available from the literature regarding the role of chirality on amyloid aggregation do not offer an univocal hypothesis on this point; i.e., chirality seems to play a role for some peptide breakers^[39] but not for some fluorine derivatives.^[40] A similar controversial case is that of nicotine for which each of the D-(+) and L-(-) enantiomers was found to inhibit $A\beta$ aggregation,^[41] while the racemate was previously found inactive.^[42] Further studies are required to fully elucidate the role of chirality on amyloid fibril formation to better clarify the mechanism of action.

As a general consideration, it can also be stated that, considering the levels of $A\beta_{1-42}$ in the cerebrospinal fluid of patients afflicted with mild cognitive impairment or sporadic AD are in the subnanomolar range,^[43,44] it is conceivable to say that the (*R*)- and (*S*)-**1** may potentially exert their antiaggregating action when a sub-nanomolar concentration in brain is reached. Moreover, on the basis of these considerations, it also seems plausible that similar amounts of inhibitor can simultaneously exert both anticholinesterasic and antiaggregating activities.

On the basis of their interesting activity profiles, the neuroprotective activity of the enantiomers and the racemate of **1** against $A\beta_{25-35}$ -induced cytotoxicity in SH-SY5Y neuroblastoma cells was investigated. Treatment of SH-SY5Y cells for 24 h with $30 \mu\text{M}$ $A\beta_{25-35}$ reduced cell viability by 42%, as measured by reduction of MTT (Figure 4). (*R*)-**1**, (*S*)-**1** and the racemic mixture were incubated at concentrations of 0.3 to $10 \mu\text{M}$, 24 h before

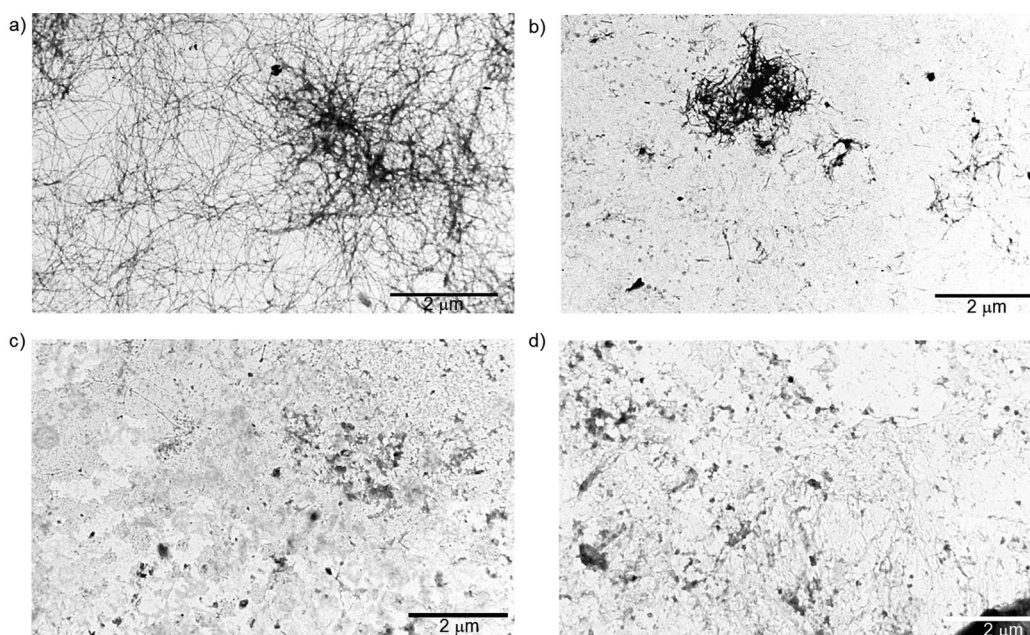


Figure 3. TEM images of $A\beta_{1-42}$ aggregates after 24 h of incubation at 30°C in the absence (a) and in the presence of (*R/S*)-**1** (b), (*R*)-**1** (c), and (*S*)-**1** (d). Samples were negatively stained with aqueous uranyl acetate solution (1%) before image acquisition. Bars = $2 \mu\text{m}$, magnification = $7900\times$.

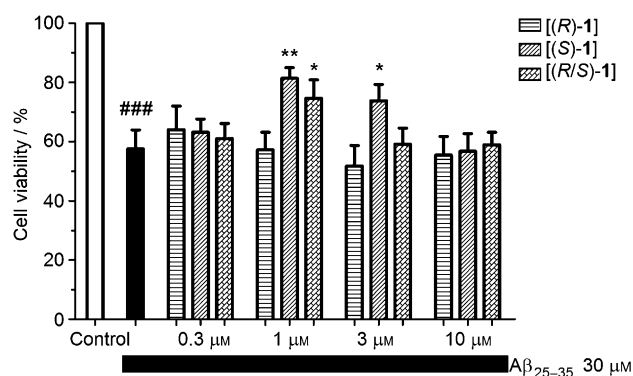


Figure 4. Neuroprotective effect of (*R/S*)-1, (*R*)-1 or (*S*)-1 against A β_{25-35} -induced toxicity in the SH-SY5Y neuroblastoma cell line. Cells were treated with (*R/S*)-1, (*R*)-1 or (*S*)-1 (0.3–10 μ M) 24 h before and during 24 h incubation with A β_{25-35} (30 μ M). After this period, cell viability was quantified by measuring MTT reduction. The control group was considered as 100% and represents cell viability of cells incubated in culture medium only. Data are the mean \pm standard error of the mean (SEM) of triplicates of four different cell batches: ### $p < 0.001$ versus control; ** $p < 0.01$ and (*) $p < 0.05$ with comparison to A β_{25-35} -treated cells in the absence of tested compound.

and during a 24 h period of exposure to A β_{25-35} . (*S*)-1 afforded significant protection against A β_{25-35} -induced toxicity when tested at 1 and 3 μ M. Maximum protection achieved with (*S*)-1 was higher than that obtained with the racemic mixture: 56% versus 39%, respectively (at 1 μ M). Conversely, (*R*)-1 did not provide protection at any of the tested concentrations. Curiously, protection by the racemate was lost at 3 μ M, and at 10 μ M of the (*S*)-1 enantiomer. Loss of protection at higher concentrations has also been described with other cholinergic neuroprotective drugs,^[45] although we cannot provide a clear explanation for this phenomenon.

Finally, to address the potential cytotoxicity of tacrine derivatives, the effects of tacrine and neuroprotective enantiomer (*S*)-1 (3–100 μ M) on cell viability was evaluated. Tacrine significantly reduced cell viability by 69% at 30 μ M, while at 100 μ M residual cell viability was only 17% (Figure 5). Conversely, (*S*)-1 was less cytotoxic, and a significant reduction in cell viability was observed only at 100 μ M (61%), a concentration 100-times higher than that needed to exert a neuroprotective effect against A β -induced toxicity.

In conclusion, on the basis of the overall activity profile, enantiomer (*S*)-1 emerged as a new promising drug candidate inhibiting cholinesterase activity, AChE-induced amyloid aggregation, amyloid A β_{1-42} self-aggregation in vitro, and exhibiting significant neuroprotection against A β_{25-35} -induced cytotoxicity. The neuroprotective effect is exerted at 1 μ M, a concentration at which cell viability is unaffected. These activities further enlarge the previously presented pharmacological profile of *p*-methoxytacrine, which was also shown to potentially cross the blood–brain barrier and act as both an antioxidant and potent calcium-channel blocker.^[18]

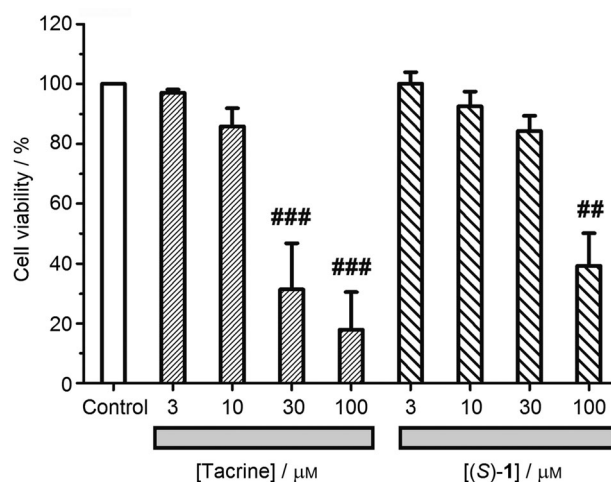


Figure 5. Cytotoxic effects of tacrine and (*S*)-1 in the SH-SY5Y cell line. Cells were incubated for 24 h with increasing concentrations of tacrine and (*S*)-1, then cell viability was assessed by measuring MTT reduction. ### $p < 0.001$ and ## $p < 0.01$ in comparison to control (cells untreated with drug).

Experimental Section

Synthesis: Reactions were monitored by thin layer chromatography (TLC) using precoated silica gel aluminum plates containing a fluorescent indicator (Merck KGaA, Darmstadt, Germany), with detection by UV light (254 nm) followed by charring with H₂SO₄/AcOH (50:50, v/v) spray, aq KMnO₄ (1%) or phosphomolybdic acid (0.5%) in EtOH (95%). Anhydrous Na₂SO₄ was used to dry organic solutions during work-up, and the removal of solvents was carried out in vacuo using a rotary evaporator. Flash chromatography was performed using silica gel 60 (230–400 mesh; Merck KGaA, Darmstadt, Germany). Melting points (mp) are uncorrected. ¹H and ¹³C NMR spectra were recorded using tetramethylsilane (TMS) as an internal standard. Reactions were performed under microwave irradiation (MWI) in a CEM Discover system single-mode microwave reactor (Biotope, Uppsala, Sweden) equipped with electromagnetic sample stirrer, an infrared temperature detector and a pressure sensor. The microwave reactions were performed in glass tubes (30 mL) equipped with septa.

(*R*)-Ethyl 5-amino-4-(4-methoxyphenyl)-2-methyl-1,4,6,7,8,9-hexahydrobenzo[*b*][1,8]naphthyridine-3-carboxylate [(*R*)-1]:^[18] mp: 109–111 °C; [α]_D = +179 ($c = 0.5$ in CHCl₃); ¹H NMR (300 MHz, CDCl₃): δ = 7.25 (d, $J = 8.7$ Hz, 2H), 6.77 (d, $J = 8.7$ Hz, 2H), 6.53 (br s, 1H, NH), 4.96 (s, 1H, H₄), 4.12 (q, $J = 7.1$ Hz, 2H), 4.02 (br s, 2H, NH₂), 3.75 (s, 3H, OCH₃), 2.69–2.65 (m, 1H), 2.36 (s, 3H, CH₃), 2.33–2.22 (m, 1H), 1.83–1.75 (m, 2H, CH₂), 1.64–1.57 (m, 2H, CH₂), 1.27 ppm (t, $J = 7.1$ Hz, 3H); ¹³C NMR (75 MHz, [D₆]DMSO): δ = 167.0 (C=O), 157.3 (C_{4'}), 151.8 (C_{9a}), 149.4 (C_{10a}), 147.8 (C₂), 146.8 (C₅), 139.7 (C_{1'}), 128.5 (C_{2'}), 113.0 (C_{3'}), 110.7 (C_{5a}), 100.0 (C_{4a}), 98.37 (C₃), 58.4 (OCH₂CH₃), 54.8 [CH₃O(C_{4'})], 36.8 (C₄), 31.8 (C₉), 22.9 (C₆), 22.4 (C₇), 22.3 (C₈), 18.9 [CH₃(C₂)], 14.2 ppm (CH₃CH₂O).

(*S*)-Ethyl 5-amino-4-(4-methoxyphenyl)-2-methyl-1,4,6,7,8,9-hexahydrobenzo[*b*][1,8]naphthyridine-3-carboxylate [(*S*)-1]:^[18] [α]_D = –180 ($c = 0.62$ in CHCl₃). Compound (*S*)-1 and its enantiomer (*R*)-1 showed identical NMR spectra.

Separation of 1 enantiomers by HPLC on a chiral stationary phase: Resolution of (*R/S*)-*p*-methoxytacrine (1) was carried out by semi-preparative high-performance liquid chromatography (HPLC) using a CHIRALPAK AD (amylose tris(3,5-dimethyl-phenyl

carbamate), 250×20 mm, 10 μm; Chiral Technologies Europe, Cedex, France) as the chiral stationary phase and MeOH/MeCN (98:2) containing dimethylethanolamine (DMEA; 0.2% v/v) as the mobile phase.^[18] Enantiomeric excess (ee) of the isolated fractions was determined using a CHIRALPAK AD (amylose tris(3,5-dimethylphenyl carbamate), 150×4.6 mm, 5 μm; Chiral Technologies Europe, Cedex, France) analytical column and MeOH/MeCN (90:10) containing DMEA (0.2% v/v) as the mobile phase. The less polar enantiomer (R)-1 showed a retention factor (*k'*) of 0.604, while the more polar enantiomer (S)-1 had a *k'* value of 1.764 (see Supporting Information in Reference [18])

Determination of the inhibitory potency on Aβ_{1–40} aggregation mediated by recombinant hAChE:^[30] Aliquots of Aβ_{1–40} (2 μL; Bachem AG, Switzerland), lyophilized from 1,1,1,3,3,3-hexafluoro-2-propanol (HFIP; 2 mg mL⁻¹) and dissolved in dimethyl sulfoxide (DMSO) at a final concentration of 230 μM, were incubated for 24 h at RT in sodium phosphate buffer (0.215 M, pH 8.0). Aliquots of hAChE (2.30 μM, molar ratio 100:1) and hrAChE in the presence of the test compound (100 μM) were added. Blanks containing Aβ alone, hrAChE alone, or Aβ plus the test compound, and hrAChE plus the test compound in sodium phosphate buffer (0.215 M, pH 8.0) were prepared. To quantify amyloid fibril formation, the thioflavin T (ThT) fluorescence method was used.^[35,36] In brief, after incubation, the samples were diluted to a final volume of 2 mL with 50 mM glycine/NaOH buffer (pH 8.5) containing 1.5 μM ThT. A 300 s time scan of fluorescence intensity was carried out ($\lambda_{\text{exc}} = 446 \text{ nm}$, $\lambda_{\text{em}} = 490 \text{ nm}$), and values at the plateau were averaged after subtraction of the background fluorescence of the 1.5 μM ThT solution. The fluorescence intensities in the absence and in the presence of the inhibitor were compared and the percent inhibition was calculated.

Determination of the inhibitory potency on Aβ_{1–42} self-aggregation: HFIP-pretreated Aβ_{1–42} samples (Bachem AG, Switzerland) were resolubilized with a MeCN/0.3 mM Na₂CO₃/250 mM NaOH (48.4:48.4:3.2) to have a stable stock solution ([Aβ_{1–42}] = 500 μM).^[46] Experiments were performed by incubating the peptide in 10 mM phosphate buffer (pH 8.0) containing 10 mM NaCl at 30 °C for 24 h ([Aβ] = 50 μM) with and without inhibitor. Stock solutions (1.5 mM) were prepared by dissolving test inhibitors in MeCN. Blanks containing test inhibitors and ThT were also prepared and evaluated to account for quenching and interference eventually related to inhibitor fluorescence. To quantify amyloid fibril formation, the ThT fluorescence method was used.^[35,36] After incubation, samples were treated as for the determination of the inhibitory potency on Aβ_{1–40} aggregation induced by hAChE.

TEM studies: Samples of Aβ_{1–42} (50 μM) with and without (R)-, (S)- and (R/S)-1 (50 μM) were prepared as reported for the determination of the inhibitory potency on Aβ_{1–42} self-aggregation. Aliquots of each sample (2.5 μL) were then adsorbed onto 200-mesh carbon-coated copper grids (Electron Microscopy Sciences, Hatfield, USA) until dryness. The grids were then washed with 0.22 μm-filtered bidistilled water (3×10 μL), stained with 1% aq uranyl acetate (Sigma, Milan, Italy) for 5 min, and finally washed further with 0.22 μm-filtered bidistilled water (3×10 μL). The grids were allowed to dry and were then visualized in a Philips CM100 transmission electron microscope (accelerating voltage 80 kV).

Molecular modeling studies

(R)-1 and (S)-1 were assembled within Discovery Studio version 2.1, software package, using standard bond lengths, bond angles and without protonation at the pyridine ring. With the CHARMM force-

field^[47] and partial atomic charges, the molecular geometries of (R)-1 and (S)-1 were each separately energy minimized using the adopted-based Newton–Raphson algorithm. Structures were considered fully optimized when the energy changes between iterations were less than 0.01 Kcal mol⁻¹.^[48] Tacrine was retrieved from the TcAChE–tacrine complex (PDB ID: 1ACJ).^[49] The coordinates of hAChE (PDB ID: 1B41^[50]), and hBuChE complexed with choline (PDB ID: 1POM^[51]) and butyrate (PDB ID: 1P0I^[51]) were obtained from the Protein Data Bank (PDB). For docking studies, initial proteins were prepared by removing all water molecules, heteroatoms, and any co-crystallized solvent and ligands (choline and butyrate). To correct for poor or missing assignments of explicit hydrogen atoms in the PDB structures, and to accommodate bond order information not possible in the PDB file format, proper bonds, bond orders, hybridization and charges were assigned using the protein model tool in Discovery Studio. A CHARMM forcefield was applied using the receptor–ligand interactions tool in Discovery Studio. Docking calculations were performed using AutoDock Vina.^[52] AutoDockTools (ADT; version 1.5.4) was used to add hydrogen atoms and partial charges for proteins and ligands using Gasteiger charges. Flexible torsions in the ligands were assigned with the AutoTors module, and the acyclic dihedral angles were allowed to rotate freely. Because Vina uses rectangular boxes for the binding site, the box center was defined, and the docking box was displayed using ADT. For hAChE (PDB ID: 1B41), a grid box of 20×26×22 with grid points separated by 1 Å was positioned at the active site gorge ($x = 116.546$; $y = 110.33$; $z = -134.181$). This box is big enough to include the PAS and the catalytic site. Trp286, Tyr124, Tyr337 and Tyr72 receptor residues were selected to keep flexible during docking simulation using the AutoTors module. Default parameters were used except “num modes”, which was set to 40. Before docking our ligands into the hAChE structure, the AutoDockVina docking protocol was validated using the four ligand–TcAChE complexes selected from PDB structures: THA (tacrine)/1ACJ; E20 (donepezil)/1EVE; GNT ((–)-galantamine)/1DX6 and AA7/2CKM; the three-dimensional structures of the four ligands were extracted from their respective complexes with AChE. Finally, the ligands were re-docked using the docking protocol. TcAChE was used because the X-ray crystal structures for the hAChE–ligand complexes were not available. The results showed that the RMSD values of the predicted and experimental poses of the ligands in the binding pocket of TcAChE are: 0.25 Å for THA, 0.80 Å for E20, 0.20 Å for GNT, and 0.72 Å for AA71536.

Neuroprotection against Aβ_{25–35}-induced cytotoxicity

Culture of the SH-SY5Y cell lines: SH-SY5Y cells were maintained in a 1:1 mixture of F-12 nutrient mixture (Ham12, Sigma–Aldrich, Madrid, Spain) and Eagle’s minimum essential medium (EMEM) supplemented with 15 nonessential amino acids, 1 mM sodium pyruvate, heat-inactivated fetal bovine serum (FBS), 10% penicillin (100 U mL⁻¹), and streptomycin (100 μg mL⁻¹). Reagents were obtained from Invitrogen (Madrid, Spain). Cultures were seeded into flasks containing supplemented medium and maintained at 37 °C in a humidified atmosphere of CO₂ (5%) and air (95%). For assays, SH-SY5Y cells were subcultured in 48-well plates at a seeding density of 1×10⁵ cells per well. Cells were treated with test compound before confluence in F12/EMEM with 1% FBS. All the cells used in this study were used at a low passage number (<13).

Incubation of test compound: To assess the neuroprotective effect of (R)-1, (S)-1 and (R/S)-1 against Aβ_{25–35} (30 μM)-induced toxicity, SH-SY5Y cells were preincubated with test compound at 0.3, 1, 3

and 10 μM for 24 h. Then, cells were co-incubated for another 24 h period with compound in the presence of $\text{A}\beta$ (30 μM).

Measurement of cell viability with MTT: Cell viability, and as such the mitochondrial activity of living cells, was measured by quantitative colorimetric assay with 3-[4,5-dimethylthiazol-2-yl]-2,5-diphenyltetrazolium bromide (MTT; Sigma–Aldrich, Madrid, Spain) as described previously.^[53] MTT was added to all wells (final concentration 0.5 mg mL^{-1}) and allowed to incubate in the dark at 37 °C for 2 h. The tetrazolium ring of MTT can be cleaved by mitochondrial reductases to produce a precipitated formazan derivative. After the 2 h period, the formazan produced was dissolved by adding 200 μL of DMSO, resulting in a colored compound whose optical density was measured in an ELISA reader at 540 nm. All MTT assays were performed in triplicate. Absorbance values obtained in untreated control cells were considered as 100% viability.

Acknowledgements

J.M.C. thanks the Instituto de Salud Carlos III (ISCIII), Madrid (Spain) [Red de Investigación cooperativa Neurovascular (RENEVAS); RD06/0026/1002], Comunidad Autónoma de Madrid (CAM) [S/SAL-0275-2006], and the Ministerio de Ciencia e Innovación (MICINN), Spain [SAF2006-08764-C02-01, and SAF2009-07271]. The present work was also supported by the Fundación Teófilo Hernando (MEC grants BFI2003-02722, SAF-2009-12150, SAF-2006-08540, SAF2006-1249 and CTQ2005-09365). The work at the University of Bologna was funded by a European FP7 grant, Bio-inspired Self-assembled Nanoenabled Surfaces (BISNES), and by the University of Bologna (R.F.O.). J.M.C. thanks Antonio G. García, Rafael León, and Mercedes Villarroya (Instituto Tecnológico Hotelero, Madrid, Spain) for their interest and support.

Keywords: Alzheimer's disease • amyloid β -peptides • chiral resolution • multi-target-directed ligands • tacriprine enantiomers

- [1] M. Goedert, M. G. Spillantini, *Science* **2006**, *314*, 777–781.
- [2] A. Castro, A. Martínez, *Curr. Pharm. Des.* **2006**, *12*, 4377–4387.
- [3] J. L. Cummings, *Rev. Neurol. Dis.* **2004**, *1*, 60–69.
- [4] E. Scarpini, P. Scheltens, H. Feldman, *Lancet Neurol.* **2003**, *2*, 539–547.
- [5] A. Cavalli, M. L. Bolognesi, S. Capsoni, V. Andrisano, M. Bartolini, E. Margotti, A. Cattaneo, M. Recanatini, C. Melchiorre, *Angew. Chem.* **2007**, *119*, 3763–3766; *Angew. Chem. Int. Ed.* **2007**, *46*, 3689–3692.
- [6] D. Muñoz-Torrero, P. Camps, *Curr. Med. Chem.* **2006**, *13*, 399–422.
- [7] L. Savini, A. Gaeta, C. Fattorusso, B. Catalanotti, G. Campiani, L. Chiasserini, C. Pellerano, E. Novellino, D. McKissic, A. Saxena, *J. Med. Chem.* **2003**, *46*, 1–4.
- [8] M. Decker, *J. Med. Chem.* **2006**, *49*, 5411–5413.
- [9] P. R. Carlier, E. S. Chow, Y. Han, J. Liu, J. El Yazal, Y. P. Pang, *J. Med. Chem.* **1999**, *42*, 4225–4231.
- [10] A. Cavalli, M. L. Bolognesi, A. Minarini, M. Rosini, V. Tumiatti, M. Recanatini, C. Melchiorre, *J. Med. Chem.* **2008**, *51*, 347–372.
- [11] M. I. Rodríguez-Franco, M. I. Fernández-Bachiller, C. Pérez, B. Hernández-Ledesma, B. Bartolomé, *J. Med. Chem.* **2006**, *49*, 459–462.
- [12] J. Sterling, Y. Herzig, T. Goren, N. Finkelstein, D. Lerner, W. Goldenberg, I. Miskolczi, S. Molnar, F. Rantal, T. Tamas, G. Toth, A. Zagyya, A. Zekany, J. Finberg, G. Lavian, A. Gross, R. Friedman, M. Razin, W. Huang, B. Kraiss, M. Chorev, M. B. Youdim, M. Weinstock, *J. Med. Chem.* **2002**, *45*, 5260–5279.
- [13] N. Toda, K. Tago, S. Marumoto, K. Takami, M. Ori, N. Yamada, K. Koyama, S. Naruto, K. Abe, R. Yamazaki, T. Hara, A. Aoyagi, Y. Abe, T. Kaneko, H. Kogen, *Bioorg. Med. Chem.* **2003**, *11*, 4389–4415.
- [14] M. Rosini, A. Antonello, A. Cavalli, M. L. Bolognesi, A. Minarini, G. Marucci, E. Poggesi, A. Leonardi, C. Melchiorre, *J. Med. Chem.* **2003**, *46*, 4895–4903.
- [15] P. W. Elsinghorst, J. S. Cieslik, K. Mohr, C. Trankle, M. Gutschow, *J. Med. Chem.* **2007**, *50*, 5685–5695.
- [16] L. Fang, D. Appenroth, M. Decker, M. Kiehnopf, C. Roegler, T. Deufel, C. Fleck, S. Peng, Y. Zhang, J. Lehmann, *J. Med. Chem.* **2008**, *51*, 713–716.
- [17] J. Marco-Contelles, R. Leon, C. de Los Rios, A. Guglietta, J. Terencio, M. G. Lopez, A. G. Garcia, M. Villarroya, *J. Med. Chem.* **2006**, *49*, 7607–7610.
- [18] J. Marco-Contelles, R. Leon, C. de Los Rios, A. Samadi, M. Bartolini, V. Andrisano, O. Huertas, X. Barril, F. J. Luque, M. I. Rodríguez-Franco, B. Lopez, M. G. Lopez, A. G. Garcia, C. Carreiras Mdo, M. Villarroya, *J. Med. Chem.* **2009**, *52*, 2724–2732.
- [19] J. A. Ciller, C. Seoane, J. L. Soto, B. Yrurettagoyena, *J. Heterocycl. Chem.* **1986**, *23*, 1583–1586.
- [20] R. Troschütz, T. Dennstedt, *Arch. Pharm.* **1994**, *327*, 33–40.
- [21] S. M. McElvain, J. P. Schoeder, *J. Am. Chem. Soc.* **1949**, *71*, 40–46.
- [22] C. C. Cheng, S.-J. Yan, *Org. React.* **1982**, *28*, 37–201.
- [23] J. Marco-Contelles, E. Perez-Mayoral, A. Samadi, C. Carreiras Mdo, E. Soriano, *Chem. Rev.* **2009**, *109*, 2652–2671.
- [24] J. Marco-Contelles, M. do Carmo Carreiras, *The Friedländer Reaction: Mechanism, Synthetic Applications and Experimental Conditions*, LAP Lambert Academic Publishing, Saarbrücken, **2010**.
- [25] P. Taylor, *NLN Publ.* **1974**, 43–44.
- [26] P. Taylor, N. M. Jacobs, *Mol. Pharmacol.* **1974**, *10*, 93–107.
- [27] E. O. Campos, A. Alvarez, N. C. Inestrosa, *Neurochem. Res.* **1998**, *23*, 135–140.
- [28] N. C. Inestrosa, A. Alvarez, C. A. Perez, R. D. Moreno, M. Vicente, C. Linker, O. I. Casanueva, C. Soto, J. Garrido, *Neuron* **1996**, *16*, 881–891.
- [29] G. L. Ellman, K. D. Courtney, V. Andres, Jr., R. M. Feather-Stone, *Biochem. Pharmacol.* **1961**, *7*, 88–95.
- [30] M. Bartolini, C. Bertucci, V. Cavrini, V. Andrisano, *Biochem. Pharmacol.* **2003**, *65*, 407–416.
- [31] N. C. Inestrosa, A. Alvarez, F. Calderón, *Mol. Psychiatry* **1996**, *1*, 359–361.
- [32] P. W. Elsinghorst, W. Hartig, S. Goldhammer, J. Grosche, M. Gutschow, *Org. Biomol. Chem.* **2009**, *7*, 3940–3946.
- [33] L. Piazzi, A. Rampa, A. Bisi, S. Gobbi, F. Belluti, A. Cavalli, M. Bartolini, V. Andrisano, P. Valenti, M. Recanatini, *J. Med. Chem.* **2003**, *46*, 2279–2282.
- [34] B. A. Yankner, T. Lu, *J. Biol. Chem.* **2009**, *284*, 4755–4759.
- [35] H. Naiki, K. Higuchi, K. Nakakuki, T. Takeda, *Lab. Invest.* **1991**, *65*, 104–110.
- [36] H. LeVine 3rd, *Protein Sci.* **1993**, *2*, 404–410.
- [37] P. Camps, X. Formosa, C. Galdeano, D. Muñoz-Torrero, L. Ramirez, E. Gomez, N. Isambert, R. Lavilla, A. Badia, M. V. Clos, M. Bartolini, F. Mancini, V. Andrisano, M. P. Arce, M. I. Rodríguez-Franco, O. Huertas, T. Dafni, F. J. Luque, *J. Med. Chem.* **2009**, *52*, 5365–5379.
- [38] M. L. Bolognesi, A. Cavalli, L. Valgimigli, M. Bartolini, M. Rosini, V. Andrisano, M. Recanatini, C. Melchiorre, *J. Med. Chem.* **2007**, *50*, 6446–6449.
- [39] N. Kokkonen, K. Stott, H. Amijee, J. M. Mason, A. J. Doig, *Biochemistry* **2006**, *45*, 9906–9918.
- [40] A. Sood, M. Abid, S. Hailemichael, M. Foster, B. Torok, M. Torok, *Bioorg. Med. Chem. Lett.* **2009**, *19*, 6931–6934.
- [41] S. A. Moore, T. N. Huckerby, G. L. Gibson, N. J. Fullwood, S. Turnbull, B. J. Tabner, O. M. El-Agnaf, D. Allsop, *Biochemistry* **2004**, *43*, 819–826.
- [42] T. Kihara, S. Shimohama, A. Akaike, *Jpn. J. Pharmacol.* **1999**, *79*, 393–396.
- [43] M. Bjerke, E. Portelius, L. Minthon, A. Wallin, H. Anckarsater, R. Anckarsater, N. Andreasen, H. Zetterberg, U. Andreasson, K. Blennow, *Int. J. Alzheimer's Dis.* **2010**, 986310.
- [44] M. Bibl, B. Mollenhauer, H. Esselmann, P. Lewczuk, H. W. Klafki, K. Sparbier, A. Smirnov, L. Cepek, C. Trenkwalder, E. Ruther, J. Kornhuber, M. Otto, J. Wiltfang, *Brain* **2006**, *129*, 1177–1187.
- [45] E. Arias, S. Gallego-Sandin, M. Villarroya, A. G. Garcia, M. G. Lopez, *J. Pharmacol. Exp. Ther.* **2005**, *315*, 1346–1353.
- [46] M. Bartolini, C. Bertucci, M. L. Bolognesi, A. Cavalli, C. Melchiorre, V. Andrisano, *ChemBioChem* **2007**, *8*, 2152–2161.
- [47] B. R. Brooks, R. E. Bruccoleri, B. D. Olafson, D. J. States, S. Swaminathan, M. Karplus, *J. Comput. Chem.* **1983**, *4*, 187–217.
- [48] A. Morreale, F. Maseras, I. Iriepa, E. Galvez, *J. Mol. Graphics Modell.* **2002**, *21*, 111–118.

- [49] M. Harel, I. Schalk, L. Ehret-Sabatier, F. Bouet, M. Goeldner, C. Hirth, P. H. Axelsen, I. Silman, J. L. Sussman, *Proc. Natl. Acad. Sci. U.S.A.* **1993**, *90*, 9031–9035.
- [50] G. Kryger, M. Harel, K. Giles, L. Toker, B. Velan, A. Lazar, C. Kronman, D. Barak, N. Ariel, A. Shafferman, I. Silman, J. L. Sussman, *Acta Crystallogr. Sect. D.* **2000**, *56*, 1385–1394.
- [51] Y. Nicolet, O. Lockridge, P. Masson, J. C. Fontecilla-Camps, F. Nachon, *J. Biol. Chem.* **2003**, *278*, 41141–41147.
- [52] O. Trott, A. J. Olson, *J. Comput. Chem.* **2010**, *31*, 455–461.
- [53] F. Denizot, R. Lang, *J. Immunol. Methods* **1986**, *89*, 271–277.

Received: May 13, 2011

Revised: July 22, 2011

Published online on August 24, 2011
